Biophysical Journal
Article

Biophysical Society

Natural Conformational Sampling of Human TNFα Visualized by Double Electron-Electron Resonance

Bruce Carrington,[1,*] William K. Myers,[2] Peter Horanyi,[3] Mark Calmiano,[1] and Alastair D. G. Lawson[1]
[1]UCB Celltech, Slough, United Kingdom; [2]Department of Inorganic Chemistry, University of Oxford, Oxford, United Kingdom; and [3]Beryllium, Bainbridge Island, Washington

ABSTRACT Double electron-electron resonance in conjunction with site-directed spin labeling has been used to probe natural conformational sampling of the human tumor necrosis factor α trimer. We suggest a previously unreported, predeoligomerization conformation of the trimer that has been shown to be sampled at low frequency. A model of this trimeric state has been constructed based on crystal structures using the double-electron-electron-resonance distances. The model shows one of the protomers to be rotated and tilted outward at the tip end, leading to a breaking of the trimerous symmetry and distortion at a receptor-binding interface. The new structure offers opportunities to modulate the biological activity of tumor necrosis factor α through stabilization of the distorted trimer with small molecules.

INTRODUCTION

Although tumor necrosis factor α (TNFα) was first discovered over 40 years ago (1) and has since become the number one drug target in rheumatoid arthritis, with biologicals such as adalimumab, infliximab, etanercept, certolizumab pegol, and golimumab transforming clinical practice (2), precise details of its structural biology and fine tuning of its activity remain elusive.

As long ago as 1987, Wingfield et al. (3) used a variety of biophysical techniques to establish that TNFα was a compact trimer, with confirmation, in the form of the crystal structure, being published two years later by Jones et al. (4). Both techniques required high concentrations of TNFα, but in 1992, Corti et al. (5) showed that TNFα structural biology was more dynamic than suggested by the crystal structures. The group used two immunoenzymatic assays (one specific for oligomeric and one specific for protomeric TNFα) to establish that trimeric TNFα is able to convert between active (trimeric) and inactive (single protomeric) forms, and that this interconversion was concentration dependent. In a follow-up study using surface plasmon resonance and enzyme-linked immunosorbent assay, measurement of dissociation rates was performed, with a half-life of 17.5–20.9 h quoted (6). Indeed at physiologically relevant concentrations (picomolar), TNFα may be expected to be predominantly single protomers, and largely inactive, with transient formation of trimers in locally high concentrations (nanomolar), pointing to a degree of fine regulation of the biological activity of the cytokine based on dynamic changes in quaternary structure. The precise mechanism of trimer/protomer interchange is still not clear, but it may offer interesting new opportunities for therapeutic intervention.

Indeed, the mechanism whereby the small molecule suramin is able to inhibit the activity of TNFα has been shown to involve deoligomerization of the trimer (7). Data from quantitative size-exclusion chromatography (SEC) with ^{125}I-labeled TNFα were best fitted to a model that involved conformational change in the trimer to stabilize a state prone to deoligomerization and favored by suramin binding. The first potential link between stabilization of a conformation prone to dissociation into dimer and protomer and inhibition of TNFα activity was also made in this article.

X-ray crystallography revealed that the compound SPD305 inhibited the biological activity of TNFα by stabilizing a dimeric conformation in which one protomer has been displaced by the small molecule (8). The authors favored a predissociation-independent model for the mechanism of binding. A similar phenomenon has been observed with a peptide macrocycle, M21, with an x-ray crystal structure revealing the bicyclic peptide bound to a dimer of TNFα and overlapping with the binding site of SPD305 (9).

The x-ray co-crystal structure of TNFα dimer bound to SPD304 has also served as a molecular model for in silico screening of a natural-product-like chemical library (10), with a pyrazole-linked quinuclidine and an

Submitted March 6, 2017, and accepted for publication June 6, 2017.

*Correspondence: bruce.carrington@ucb.com

Editor: Elizabeth Rhoades.
http://dx.doi.org/10.1016/j.bpj.2017.06.007

indolo-quinolizidine scaffold emerging with binding poses unsurprisingly similar to those for SPD304. Stabilization of the inactive dimeric form by compounds discovered through virtual screening has also been the approach of Choi et al. (11).

We have been interested in achieving clinical effects similar to those achieved with the TNFα biologicals, but with small molecules, to address issues of immunogenicity (12,13), supply chain complexity (14), health economics, and other indications e.g., a TNFα inhibitor with an anti-amyloid β could slow the progression of Alzheimer's disease (15). The opportunity to fine-tune TNFα biology with small molecules could also increase the therapeutic safety window over infection risk. We wanted to see if it was possible to define structurally a conformation of TNFα that was predeoligomerization (before protomer loss) but in a state that predisposed the molecule to deoligomerization, and to see if this conformation was naturally sampled at sufficient frequency to be considered a druggable conformation for a small molecule.

Inspired by the literature on atomic-distance measurement in proteins (16) and by identification of a conformational ensemble of the outward- and inward-facing states of the transmembrane trimer of the sodium-coupled aspartate transporter using double electron-electron resonance (DEER) (17,18), we decided to apply DEER to the TNFα trimer in solution in an attempt to reveal natural sampling of one or more defined intermediate conformations before actual protomer loss.

DEER as a technique is well suited to the elucidation of protomer movement within a trimer, as only one residue needs to be labeled to obtain three interprotomer distances. If the trimer is displaying trimerous symmetry, then the distance distributions plotted from interpretation of the dipolar interactions will be a sharp, single peak corresponding to identical distances between the spin label on each protomer. Distortion of the trimer caused by movement of one protomer relative to the others will manifest in the appearance of additional peaks. Integration of these peaks can indicate the percentage of trimers sampling different conformations at any time, and new working models, based on crystal structures but adapted to accommodate distance measurements from DEER, can be generated to gain insight into trimer conformational sampling. A new area of computational biology is emerging to fit ensembles of conformers to DEER distance distributions (19).

Labeling sites on human TNFα were selected from analysis of crystal structures to provide representation of protomer movement at two positions, one toward the N/C-terminal end of the trimer, which is well defined by crystallography, and one toward the tip, a more flexible region.

Analysis of the DEER measurements using molecular modeling data indicates a biophysical structural basis for conformational sampling within the intact trimer, a mechanism by which protomer loss can occur, and an opportunity to use a small molecule to stabilize a predeoligomerization, signaling-incompetent state of TNFα.

MATERIALS AND METHODS

Plasmid constructions TNF-T77C and TNF-I83C

A plasmid encoding human TNFα (UniProt: P01375, residues 77–233) was used as a template to clone TNF-T77C. The template gene was codon engineered for *Escherichia coli* expression in silico using GeneComposer and optimized to balance GC content, to exclude cryptic Shine Dalgarno sequences, and to exclude BamHI and *Hin*dIII restriction sites. To generate TNF-T77C, the previously described plasmid template was used with primers annealing to bases corresponding to human TNFα residues 77–233 and which incorporate the sequence GGATCC (BamHI) on the 5′ end and TGATAAGCTT on the 3′ end, resulting in a polymerase chain reaction product with unique BamHI and *Hin*dIII sites. Additional bases ATATAT were incorporated via the same primers on the 5′ and 3′ termini of the product to facilitate efficient digestion of the polymerase chain reaction product. After confirmation of the expected size fragment on a 1% agarose gel, the fragment was digested with BamHI/*Hin*dIII, gel purified, and subcloned into gel-purified BamHI/*Hin*dIII-digested vector pEMB54, which is an ampicillin-resistant, arabinose-inducible vector with pMB1 origin of replication and 6XHis-*Smt3* (yeast *Smt3*, Uniprot: Q12306, residues 17–98) under the PBAD promoter. Vector pEMB54 contains unique BamHI and *Hin*dIII sites after the His-*Smt3* sequence, such that after BamHI/*Hin*dIII subcloning, the gene of interest is fused in frame on the N-terminus with 6XHis-*Smt3*. A portion of the resulting ligation was transformed to chemically competent TOP10 cells, plated on 10 cm 2YT agar plates containing 100 μg/mL ampicillin, and incubated overnight at 37°C. One transformant was miniprepped and the DNA was sequence verified over the open reading frame. Site-directed mutagenesis was carried out using the Quik Change II Site-Directed Mutagenesis Kit (Agilent, Santa Clara, CA) to mutate threonine 153 to a cysteine. The resulting DNA was transformed to chemically competent TOP10 cells, plated on 10 cm 2YT agar plates containing 100 μg/mL ampicillin, and incubated overnight at 37°C. One transformant was miniprepped and the DNA was sequence verified over the open reading frame.

Human TNFα (residues 77–233, I159C) TNF-I83C was generated in the same manner; however, site directed mutagenesis was carried out to mutate isoleucine 159 of the tagged construct to a cysteine.

Fermentation of human TNFα (77–233, T153C) TNF-T77C and human TNFα (77–233, I159C) TNF-I83C to generate the perdeuterated reagent

The target-specific vector was transformed (fresh transformation) into BL21 (DE3) *E. coli* cells. A starter culture containing 100 μg/mL (final concentration) ampicillin in Terrific Broth was inoculated with a single colony and grown, with shaking, at 37°C until it reached an OD_{600} of 0.71, at which time the culture was transferred to 4°C overnight. The next day the cells were pelleted, resuspended in a 10× volume (160 mL) of the original culture volume in M9/H_2O media (20) and grown, with shaking, to an OD_{600} of 0.6. The cells were aliquoted (20 mL aliquots) and pelleted, and each aliquot was resuspended in 100 mL of M9/D2O with D-[2H]-glucose media in a sterile 2 L flask. Cultures were grown, with shaking, at 37°C until an OD_{600} of 0.4 was reached. Two hundred milliliters of prewarmed M9/D2O with D-[2H]-glucose media was added to each flask and grown, with shaking, at 37°C until an OD_{600} of 0.4 was reached. Then, an additional seven hundred milliliters of prewarmed M9/D2O with D-[2H]-glucose media was added to each flask and grown at 37°C until an OD_{600} of 0.4 was reached. The cultures were then induced with arabinose (final concentration of 1%) and incubated at 37°C for 12 h until a final OD_{600} of 1.2 was reached. The cells were harvested by centrifugation

(Beckman-Coulter, Fullerton, CA) at 5000 rpm for 15 min, and the pellets were collected and immediately purified.

Fermentation of the TNF T77C construct for crystallography was performed in the same manner as for generation of the perdeuterated protein for DEER, except that nondeuterated reagents were employed.

Purification and spin labeling of human TNFα (77–233, T153C) TNF-T77C and TNFα (77–233, I159C) TNF-I83C

The reagents for cell culture were snap frozen in LN_2 before lysis to allow one freeze-thaw cycle. Cells were resuspended at 1 g:5 mL in 25 mM Tris (hydroxymethyl) aminomethane hydrochloride (Tris-HCl) (pH 8.0), 200 mM NaCl, 0.5% 3-((3-cholamidopropyl) dimethylammonio)-1-propanesulfonate, 50 mM L-arginine, 250 U of benzonase, 100 mg lysozyme (Sigma-Aldrich, St. Louis, MO), and one cOmplete EDTA-free protease inhibitor tablet (Roche, Basel, Switzerland). The cells were lysed via sonication (Misonix, Farmingdale, NY) on ice, clarified via centrifugation at 42,000 rpm for 30 min at 4°C (Beckman Coulter), and filtered with a 0.8–0.2-μm gradient filter (Pall, Port Washington, NY). The supernatant was applied to three 1 mL Ni^{2+} charged HiTrap chelating high-performance columns (GE Healthcare, Little Chalfont, United Kingdom) and the protein was eluted within a 500 mM imidazole gradient over 40 column volumes. The fractions of interest were pooled and the His-Smt tag was removed via cleavage with ubiquitin-like-specific protease 1 (Ulp-1) while dialyzing against 2 L of 25 mM Tris (pH 8.0) and 200 mM NaCl overnight at 4°C utilizing 10 kDa molecular-weight cutoff (MWCO) snakeskin dialysis tubing. The affinity tag was removed by applying the digested pool over one 5 mL Ni^{2+} charged HisTrap fast-flow column (GE Healthcare). The flowthrough contained the cleaved protein of interest. This pool was concentrated for labeling and SEC via centrifugal concentration (Vivaspin polyethylsulfone, 10 kDa MWCO; Sartorius, Bohemia, NY) to 7.7 mg/mL and was labeled by reconstituting 100 mg of 3((methanesulfonylsulfanyl) methyl)-2,2,5,5-tetramethyl-2,5-dihydro-1H-pyrrol-1-olate (MTSSL) (Fig. 1) in dimethylsulfoxide (DMSO). The reconstituted label was combined with the purified concentrated digested pool and incubated overnight at 4°C with nutating away from light. The final labeling volume was 3 mL with 22 mg of protein (in 2.8 mL of 7.7 mg/mL protein solution and 200 μL of 100 mg spin label) and 100 mg of spin label. The molar ratio was 135 mM:414 μM MTSL/perdeuterated TNFα, or 305:1. The supernatant was injected over a HiLoad 16/60 Superdex 200 PG (GE Healthcare) in 10 mM HEPES (pH 7.5) and 150 mM NaCl. Fractions of interest were pooled, buffer exchanged, and concentrated into 10 mM potassium phosphate (deuterated), 150 mM NaCl, 30% v/v glycerol-d8 (pH 7.5), and 100% D_2O at a concentration of 7.65 mg/mL (440 μM), and stored at −80°C. The efficiency of labeling was >90% by continuous-wave electron paramagnetic resonance (CW-EPR).

Purification and spin labeling of the protein for crystallography was performed in the same manner as for generation of the perdeuterated protein for DEER, except that nondeuterated reagents were employed and the final buffer of the protein was 10 mM HEPES (pH 7.5) and 150 mM NaCl.

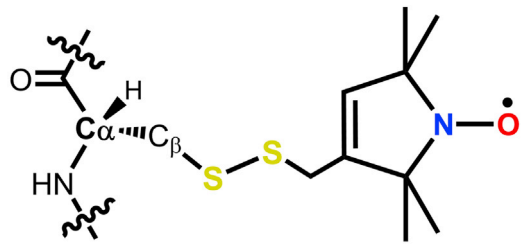

FIGURE 1 Structure of MTSSL attached to a cysteine side group.

Crystallization and structure determination of spin-labeled human TNFα (77–233, T153C) TNF-T77C-MTSSL

TNFα (T77C mutant spin labeled with MTSSL) at 10 mg/mL (in 10 mM HEPES (pH 7.5) and 150 mM NaCl) was mixed with an equal volume of crystallant solution containing 24% (w/v) PEG-4000, 0.24 M $MgCl_2$, 0.05% n-dodecyl-β-D maltoside, and 0.1 M HEPES/NaOH (pH 8.5). Crystals were produced by sitting-drop vapor diffusion at 16°C. Crystals were then soaked with the mother liquor supplemented with 10 mM MTSSL in DMSO for 1 week and harvested in paraffin oil, and the data were collected at APS 21-ID-F at a wavelength of 0.97872 Å. The data were reduced using XDS (21), structure refinement was performed in Phenix (22), and the model was modulated in COOT (23).

X-band CW-EPR spectroscopy

CW-EPR measurements were performed in the Centre for Advanced ESR (CAESR) in the Chemistry Department of the University of Oxford, using an EMX microspectrometer for CW-EPR characterization with a Bruker (Billerica, MA) BioSpin SHQE-W TE_{011}-mode cylindrical resonator. The two MTSSL-labeled TNFα (10 μM) samples were measured at room temperature. Nonsaturating acquisition conditions were found at a microwave frequency of 9.7807 GHz, with a microwave power of 2 mW, a field sweep of 180 G in 42.98 s, and a modulation amplitude of 0.1 mT at a frequency of 100 kHz.

Q-band DEER spectroscopy

EPR measurements were performed in CAESR in the Chemistry Department of the University of Oxford, using a Bruker BioSpin E580 spectrometer for DEER. All pulses in Q-band ELDOR were formed with an Arbitrary Waveform Generator (Bruker SpinJet AWG, SP Devices (Linköping, Sweden) SDR14) and a dielectric $TE_{01\delta}$ resonator, Bruker EN 5107D2. The microwave amplifier was an Applied Systems Engineering model 187Ka traveling wave tube amplifier (model 8922HP-1 TWT, L3 Electron Devices, Torrance, CA) with a specified $P_{sat} = 186$ W output power at 33.85 GHz. Temperature was maintained at 50 K with an Oxford Instruments (Abingdon, United Kingdom) CF935O cryostat and an Oxford Instruments Mercury instrument temperature controller. DEER data were acquired with the four-pulse sequence, $[\pi/2_{obs}] - (\tau_1) - [\pi_{obs}] - (\tau_1 + T) - [\pi_{pump}] - (\tau_2 - T) - [\pi_{obs}] - \tau_2 - <echo>$, where the observer pulses (obs) and pump frequency pulse (pump) typically had pulse lengths of 12 ns, but these occasionally varied up to 16 ns depending on resonator bandwidth restrictions. The obs frequency was most often 33.800 GHz and the pump frequency was at +100 MHz from obs and centered at the maximum of the EPR spectrum, detected by integrating the field-swept FID of an 800 ns π-pulse (24). Time delays were τ_1, the primary echo delay, τ_2, the refocused echo delay, and $T = -t_s + \sum_i^n \delta_t$, with t_s, the pump time offset before the primary echo, δ_t being the time-step increment of the experiment. The pulse sequence had a phase cycle of either 16 steps of the first two pulses (25) or an increase to 64 steps including phase cycling of the refocusing observer pulse (26), shown in Table S1. DC leakage in the pump pulse formation was minimized by adjustments to phase and amplitude offset calibrations of the SpinJet AWG. The protein was perdeuterated as expressed and diluted to a concentration of 10 μM with a buffer containing 30% glycerol-d8 and overall >50:1 $^2H/^1H$ content. The typical DEER acquisition time was 3 h. Time-domain DEER data were truncated to remove (2 + 1) artifacts at the end of the time trace (16,27); this and subsequent processing used the DeerAnalysis 2016 software (28) operating in a MATLAB R2015b environment (The MathWorks, Natick, MA).

RESULTS

Selection of labeling sites on TNFα for DEER spectroscopy

Based on the PDB: 1TNF published structure (29), residues I83 and T77 were selected as positions on the crystal structure of human TNFα suitable for representing the movement of protomers; the β-strands were well defined, and the residue side chains pointed outward to the solvent, allowing for undisturbed spin-label orientation. The C_α intratrimer distances were well within the range over which DEER is most efficient (Fig. 2), which is typically 18–80 Å. This distance range may be extended depending on spin-label type (e.g., TAM-MTS (30), bifunctional MTSSL (31), and maleimide-DOTA (Macrocyclics, Plano, TX)), the available pump pulse excitation bandwidth required to excite the entire dipolar frequencies, both primary dipolar frequencies and higher-frequency intermodulation products, and $^2H/^1H$ isotopic replacement in the protein and spin labels to suppress nuclear spin diffusion contributions to the phase memory time (16,32).

Both I83C and T77C mutants were cloned, expressed in perdeuterated media, purified, and labeled with MTSSL ((1-oxyl-2,2,5,5-tetramethyl-Δ3-pyrroline-3-methyl) methanethiosulfonate spin label). Apo TNFα (55,369 Da), T77 (53,462 Da), and I83 (54,878 Da) were trimeric by SEC with multiangle light scattering, and no aggregates were observed (Fig. S1). DEER distances are measured between N-O groups.

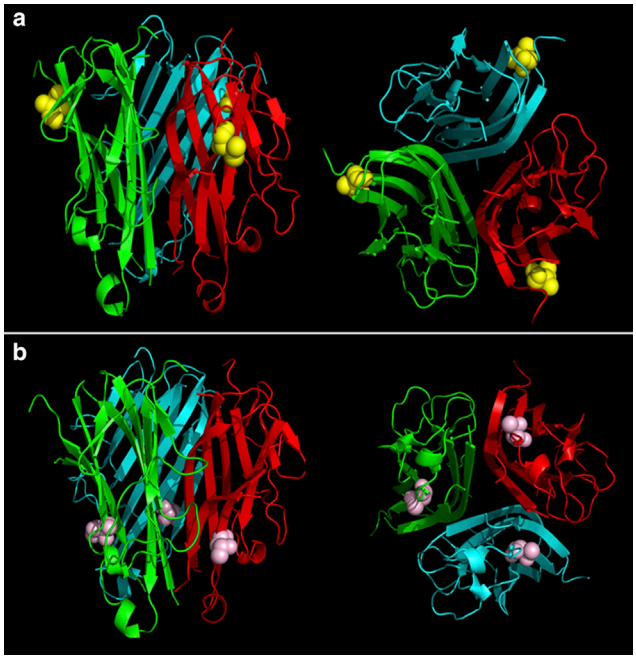

FIGURE 2 Positions of the two residues I83 (*a*) and T77 (*b*) on TNFα that were substituted with cysteines for labeling with MTSSL (PDB: 1TNF). In (*a*), I83 is shown in yellow, and in (*b*), T77 is shown in pink.

The 1.4 Å resolution crystal structure of TNFα MTSSL spin labeled on residue 77

The crystal structure of T77C mutant of TNFα labeled with MTSSL was determined to confirm that the protein structure was being undisturbed by the presence of the spin label (Fig. 3). Table 1 lists the data collection and refinement statistics. The space group was R3 and the asymmetric unit contained a single spin-labeled TNFα protomer. The trimer of TNFα is formed by three crystallographic-symmetry-related asymmetric units. In this structure, residues 69–73 and 101–110 were disordered and therefore were not modeled.

The structure was determined using Phaser (33) with a single chain of PDB: 1TNF as the search model for Molecular Replacement. The resulting solution was refined and validated in Phenix (22) and the model was fitted to the density using COOT (23).

The presence of the spin label was evident in the density with the backbone and the disulphide bond was well ordered and visible. The MTSSL side chain is highly mobile, as indicated by the increase in B-factors from 10 $Å^2$ on the backbone to 30 $Å^2$ for the sulphurs of the disulphide and 50–60 $Å^2$ for the nitroxide. It is noteworthy that the nitroxide portion of the side chain of the spin label is within 5 Å of Glu127 of a neighboring molecule in the crystal lattice, therefore potentially contributing to the partial ordering of the spin label. The occupancy of MTSSL is refined to 88% in the depicted conformation with no visible alternative conformations.

X-band CW-EPR does not detect TNFα probe steric hindrance

Room-temperature CW-EPR of both of these spin-label positions shows rotational correlation times between 1.5 and 3 ns, consistent with little steric restriction and significant interlabel orientation distributions at room temperature (Fig. S2).

Q-band DEER-distance distribution of T77C locates a second peak at +4.5 Å

DEER distance distributions were processed using the DeerAnalysis 2016 program operating in MATLAB

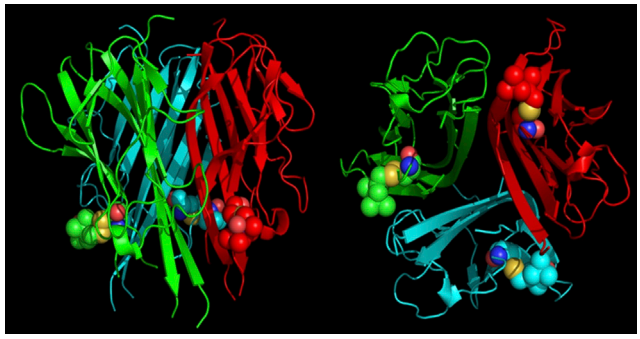

FIGURE 3 Crystal structure of MTSSL-labeled T77C apo-TNFα at 1.4 Å resolution (PDB: 5UUI).

TABLE 1 Data Collection and Refinement Statistics for the Structure PDB: 5UUI

TNFα-Apo_MTSSL[a]	
Wavelength (Å)	0.97872
Resolution range (Å)	32.83–1.4 (1.43–1.4)
Space group	R 3:H
Unit cell	65.66 65.66 84.09 90 90 120
Total reflections	98726 (5492)
Unique reflections	26091 (1816)
Multiplicity	3.8 (3.1)
Completeness (%)	97.96 (91.8)
Mean I/σ (I)	12.73 (2.29)
R-merge	0.06443 (0.4664)
R-meas	0.07438
CC1/2	0.996 (0.616)
CC*	0.999 (0.873)
R-work	0.139
R-free	0.17
Number of nonhydrogen atoms	1080
Macromolecules	1028
Water	52
Protein residues	134
RMS (bonds)	0.011
RMS (angles)	1.59
Ramachandran favored (%)	98
Ramachandran outliers (%)	0
Clashscore	5.96
Average B-factor	16.8
Macromolecules	16.6
Solvent	20.8

[a]Statistics for the highest-resolution shell are shown in parentheses.

R2015b (28) (Fig. S4). The data were treated with the ghost peak suppression algorithm of multispin effects from the intermodulation of DEER frequencies, assuming three spin labels, and the modulation depth change typically amounted to from 70% without suppression to 45% with suppression (34). For example, the peak at 24 Å (*i*) in Fig. 4 *b*, is strongly suppressed by the ghost peak suppression postprocessing, which indicates the likelihood that the peak originates from dipolar frequency intermodulation (Fig. S3).

At position 77, the DEER distance distribution with apo-TNFα gave a sharp peak (Fig. 4 *b*, *ii*) corresponding to 31 Å, but in addition, a second, less intense peak at 35.5 Å (Fig. 4 *b*, *iii*) followed by a third peak at 40 Å. The longer additional distance is not a consistent result when acquisition conditions are changed, and validation tests in DeerAnalysis show the 40 Å distance to vary to zero probability in all data sets (Fig. S4 *c*). Conversely, the 35.5 Å distance is retained in these tests. By pooling probabilities of the validation tests of nine data sets in DeerAnalysis using Eq. S1, the distance at 35.5 Å is a significant contribution within two standard deviations, as seen in the inset of Fig. 4 *b* (35). The effect of including the peak on the fit of the time-domain data may be compared across the data sets that vary in signal/noise ratio (SNR) between 45 and 180 (Fig. S5). The improvement in the χ^2 fit is at most a factor of 3 for data sets of high SNR. Integration of the peaks suggested that TNFα was spending ~94% of the time in perfect trimerous symmetry and ~6% of the time sampling a state in which a protomer or protomers were moving relative to another protomer or protomers. This movement was manifest in an increase in interprotomer distance of 4.5 Å (Fig. 4). Addition of DMSO is known to induce dissociation of the trimer, but these features are retained at up to 4% (Fig. S6). Beyond this point, trimer dissociation is known to occur.

At position 83, the DEER distance distribution with apo-TNFα gave a single, sharp peak (Fig. 4 *b*, *iv*) corresponding to 48 Å (as the crystal structure), indicating trimerous symmetry and stability of the trimer at this point. However, there was no resolution of different relative protomer conformations (Fig. 4).

Model of a potential predeoligomerization conformation of TNFα

DEER indicates that a small population of apo-TNFα exists with an interprotomer distance of 35.5 Å, an increase of +4.5 Å over the symmetric trimer at the tip end. We have attempted to model this DEER-observed conformation based on the apo crystal structure. To illustrate any conformational change to the TNFα trimer based on DEER measurements, we modeled interprotomer distances through a plane of the TNFα trimer at T77 and I83. We took a plane through the trimer, as modifying just the interprotomer T77 and I83 distances would only affect one strand on one β-sheet of each TNFα protomer, which would not reflect the true distorted nature of the TNFα conformation indicated by DEER. In the modeled structure, we make the assumption that interprotomer distances for Ile97, Ile136, Val150, Ala18, Pro117, and Val62 reflect the DEER distance distribution measured for T77. Interprotomer distances for Lys90, Asp130, Val50, Leu126, Gly54, and Leu157 then reflect the DEER distance distribution measured for I83.

A constrained minimization of the apo structure was carried out using MacroModel from Schrödinger (36) and the OPLS3 force field. At the I83 plane, interprotomer distances were constrained to the apo distances. At the T77 plane, interprotomer distances were constrained to the apo distances for two of the protomer interfaces; for a third protomer interface, the distance was increased by 4 Å over apo to reflect the DEER measurements.

The resulting constrained, minimized structure of TNFα is illustrated in Fig. 5.

DISCUSSION

DEER has been applied to the study of conformational sampling of the human TNFα trimer in solution. Structural changes in TNFα have been alluded to, but not described,

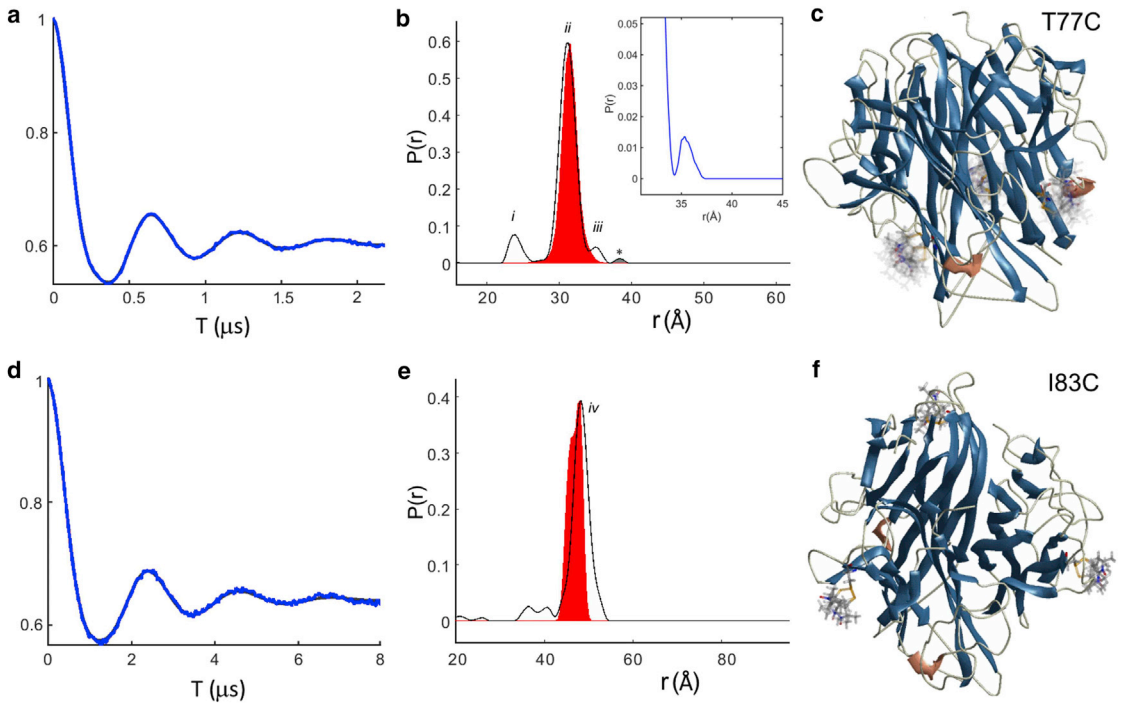

FIGURE 4 Q-band DEER measurements of T77C (*a* and *b*) and I83C (*d* and *e*) human TNFα. Form factor (*blue*) and fit (*black*) are in (*a*) and (*d*), and the distance distribution is in (*b*) and (*e*). Rotamers calculated in MMM from PDB: 5UUI are shown for T77C and I83C in (*c*) and (*f*), respectively, and P(r) values calculated in MMM are shown by red solid peaks in (*b*) and (*e*). The inset in (*b*) is the -2σ standard deviation pooled from nine data sets (35). Peaks labeled *i–iv* are discussed in the main text. Acquisition conditions are in Materials and Methods.

for intrinsic dynamic "breathing" between the TNFα protomers (37), and for conformational transitions known to precede the dissociation of the trimeric molecule (7). The stable interaction between TNFα protomers in the trimer is due to two β-strands at the protomer interface contacting almost every other residue. One edge of each subunit is packed against the inner sheet of the interacting protomer, forming large and mostly hydrophobic interfaces. Additionally, there are hydrophobic interactions between Tyr59, Tyr119, and Tyr151 of one protomer and the Phe124 of the interacting protomer (29). In addition, TNFα has been shown to be stabilized by therapeutic antibodies (38,39) and TNF receptors (40) preventing protomer exchange (41,42).

To investigate the structural changes in the TNFα trimer, two MTSSL probes were chosen, one toward the N/C-terminus at position I83 and the other near the tip end at position T77 on the same β-strand. The MTSSL TNFα crystal structure of T77 was determined to a very high resolution of 1.4 Å. Comparison between the MTSSL structure at protomer level and the PDB: 1TNF structure shows that there is 0.52 Å root mean-square deviation over 115 residues between the two structures. When the trimers are compared, the root mean-square deviation increases to 0.78 Å, demonstrating close to identical structures even at the trimer level. The new structure (PDB: 5UUI) demonstrates a folded protein in overall the same fold and oligomeric state as in the previously reported PDB: 1TNF. The crystal structure demonstrates that the presence of the spin label did not alter the protein conformation. The crystal structure gives no hint of the +4.5 Å conformation.

Room-temperature X-band CW-EPR data determined that the I83 and T77 probes are consistent with little steric restriction when bound to the β-strand. In Fig. 4, *c* and *f*, the lack of steric restriction is presented in the population of spin-label side-chain rotamers as calculated with the program Multiscale Modeling of Macromolecules (MMM). The rotameric distance distribution full width at half-maximum is remarkably close to the experimental distance distribution, supporting the use of rotamer libraries (43,44). The DEER distance distributions cannot resolve more than a single interprotomer peak at 48 Å for I83, indicating a stable protomer conformation toward the N/C-terminus of the trimer. The distances of 31 Å in T77C and 48 Å in I83C are within 1 Å of distance-distribution maxima derived from rotamer calculations with MMM (43). A peak was located at 24 Å for T77 in Fig. 4 *b*, which is strongly suppressed in the effect of the ghost peak suppression postprocessing, which indicates the likelihood that the peak originates from dipolar frequency intermodulation, Fig. S3. Extensive SEC, with or without multiwavelength light scattering, did not detect aggregates or dimerization of trimers. In the range-selective analysis of the MMM rotameric calculations, the peak at 24 Å was not populated by way of rotamers, as summarized in Table S2. To explain

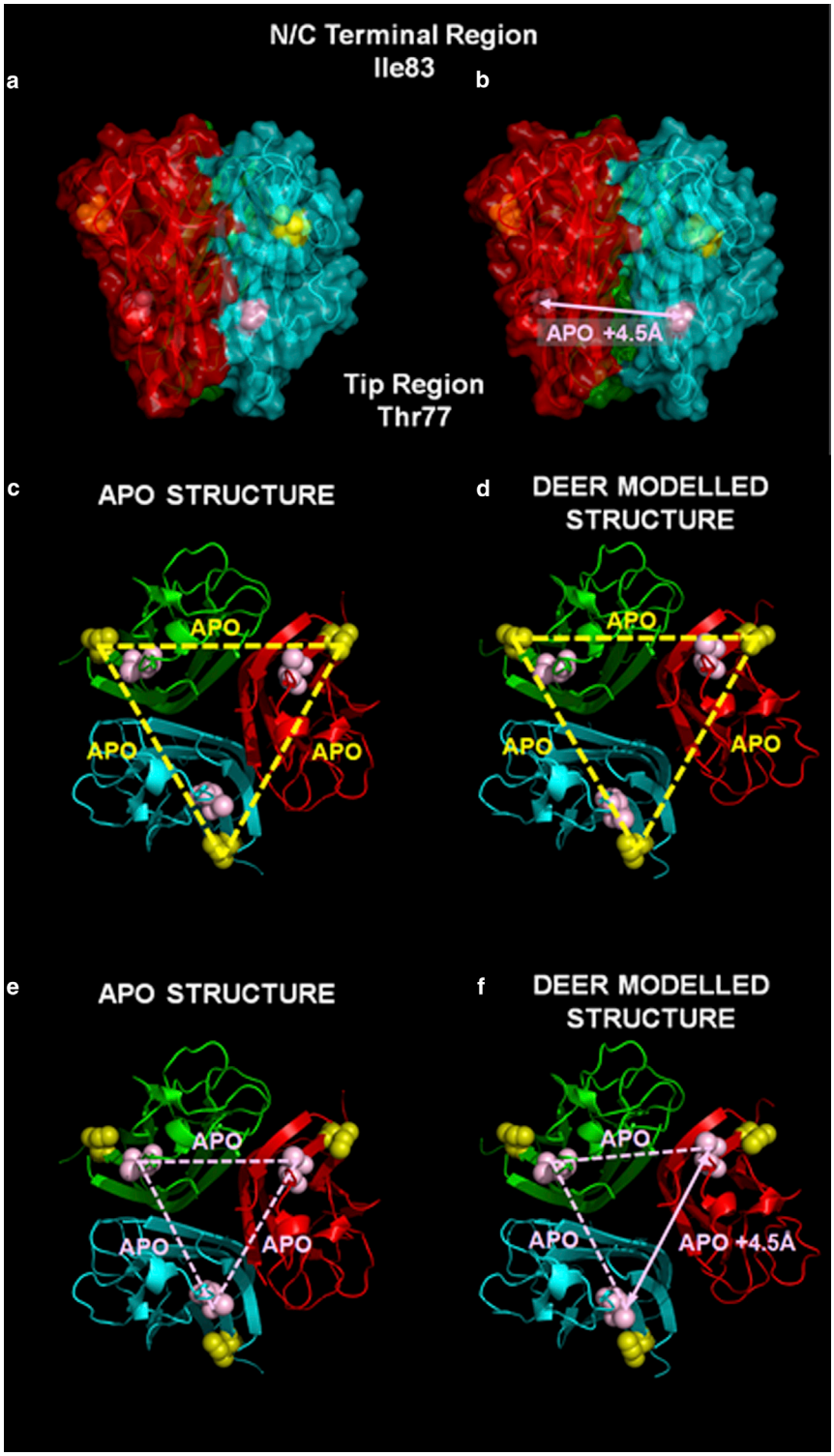

FIGURE 5 New model of TNFα showing a predeoligomerization conformation revealed by DEER, with protomer A in cyan, protomer B in green, and protomer C in red viewed from the tip region. T77 residues are highlighted in pink and I83 residues are highlighted in yellow. The 4.5 Å increase in distance between T77 positions at one interface is shown by the arrows in (*b*) and (*f*). In (*c*)–(*f*), dotted lines indicate apo distances and the solid line indicates the DEER-modeled distance, which differs from apo.

the shorter distance as an alternate spin-label side-chain conformation, one possibility would be a tucked conformation inside the trimer structure or interface paired with protomer rotation. However, a mutant shifted by one β-strand closer to the protomer interface, I97C, had a strongly immobilized component in CW-EPR proportional to a shorter distance (data not shown), which is not seen in CW-EPR of T77C.

In addition to the main peak, a small additional peak at 35.5 Å for T77 was consistently seen. In the MMM rotamer calculations (limited to spin-label pairs in MMM version 2017.1) for the distance range of 34–36.6 Å, which includes

only the peak, 0.6% of 235 distance pairs contribute, which compares to 98.9% of 12,135 pairs contributing for the range 28–34 Å. These values are different than experimentally derived distance distributions, where typical contributions of the 35.5 Å peak and main peak at 31 Å are 6.2 (± 0.9) and 93.8 (± 0.9) %, respectively, when taken together as unity for the distribution. Furthermore, this distance range is limited to 36.6 Å because of the maximum distance of the MTSSL-TNFα PDB: 5UUI model. The experimental distance extends beyond this range (Fig. S7). When all nine data sets are considered individually and when combined (Fig. S8), the -2σ level of the distribution probability leads to a discrete peak at 35.5 Å, whereas the mean and $+2\sigma$ level of the distribution are less well resolved and suggest the possibility of a continuum of protein conformers. The crystal structure of the spin-labeled TNFα molecule reveals a β-sheet with a spin label emanating in its middle without a place for stabilizing the spin label. Therefore, the infrequently sampled state was not explained by the structure and modeling used to provide insight into the potential conformation of the protein at a potentially higher energy state.

Possible reasons why the distorted form of TNFα was not detected by crystallography are that there was insufficient quantity (6%), compared to the nondistorted TNFα, to form a discrete crystal, and that the distorted form represents a higher energy state that collapses back to apo trimer structure in a crystal lattice. The distorted quaternary structural assemblies are in dynamic equilibrium, and this has been predicted to be detrimental to the solution of a protein crystal structure (45). Furthermore, Freed et al. (46) suggest that the equilibrium of substates is altered by osmolytes, e.g., PEG in the crystallization buffer, which favors the more compact, less hydrated substate to form protein crystals.

The distance between alternative conformations of the spin label in the crystal structure (PDB: 5UUI) did not account for the 35.5 Å distance detected by DEER without protein-domain movement, particularly when the sharpness of the main peak was taken into consideration. The DEER distance data have been used to construct a new model of a distorted TNFα trimer, which suggests that one protomer interface in the trimer is distorted. The model chosen with one interface at +4.5 Å was the simplest to fit the data. This does not preclude that two or all three interfaces are +4.5 Å. However, if all three interfaces opened by +4.5 Å, then the frequency would decrease threefold to 2%, as DEER distance distributions have been shown to be quantitative (47). The model shows the flexibility of TNFα protomers with rotation and outward tilting relative to the other two protomers, to form a less compact, more hydrated form of TNFα.

It is not known what role the +4.5 Å distortion has on TNFα stability, although it is suspected that this form could represent a predeoligomerization state. DEER has shown TNFα movement toward the tip region, which, rather than the N/C-terminus, is the key region for the formation of the trimeric human TNFα (48). Marušič et al. (49), using chaotropic agents, postulated an intermediate form of trimeric TNFα that was lost as the concentration decreased, leading to protomer loss. Additionally, deoligomerization can result in multimeric aggregates (40). Instability of TNFα, ascribed to TNFα dissociating during sampling, storage, and freeze thawing, may contribute to variable assay results (50). Deoligomerization can be prevented by chemical cross-linking (51), or physical linking (52).

The precise binding mechanism (53) and stoichiometry of the TNFα interaction with its receptor protein, TNFR1, are controversial (54,55) and there is a TNFα:TNFR1 reorganization upon TNFα binding, which may affect further ligand-receptor interactions (56). It is not known what role the distorted form of TNFα has on stabilization by soluble receptors. The nondistorted form of TNFα binding to TNFR1 slows down the protomer dissociation by stabilizing its trimeric structure, preventing deoligomerization and preserving its activity (40). The conformational plasticity of TNFα has led to TNFα being described as a morpheein (57). Enzymes in this class also undergo kinetic hysteresis, where turnover triggers dissociation, conformational change, and reassembly to a form with altered activity. However, morpheeins tend to have hydrophilic interfaces, and the conformational change is activating (58), whereas in TNFα, the interfaces are hydrophobic and deoligomerization is inactivating. The model of TNFα proposed in this study undergoes a rotation and tilting of a protomer, so that a predeoligomerization trimer may be incapable of binding three TNFR1 receptors and thus incapable of signaling efficiently.

It has been suggested that the structural and biophysical effects of TNFα protomer dissociation and association are linked to the physiological function to maintain TNFα homeostasis in its active trimerous form. Protomer loss can lead to multimerization, with the higher oligomers acting as a reservoir of TNFα protomers. This mechanism could tightly regulate the biological activity of TNFα at physiological concentrations (59). However, large differences in TNFα half-life occur between volunteers and patients with an activated immune system. The $T_{1/2}$ of TNFα is 8 h with patients (60), which may be due to the large excess of TNFR1 (∼300-fold) and TNFR2 (∼500-fold) over TNFα in rheumatoid arthritis patients (61).

To our knowledge, the new conformation of TNFα described here indicates that the likely entry point for stabilizing compounds, such as SPD304 and suramin, is toward the TNFα tip region. Suramin and SPD304 increase the rate of protomer dissociation by ∼6-fold. This region is also targeted by anti-TNFα therapeutic stabilizing antibodies (38,39). The approach of allosteric modulation to shift the oligomerization equilibrium has been described for peptides (shiftides) by Gabizon (62). The stabilization

of multiprotomers has been used in biologicals e.g., the insulin hexamer is stabilized by phenol and zinc (63), and Tafamidis, a drug for the amelioration of familial amyloid polyneuropathy, kinetically stabilizes the tetramer transthyretin (64). Similar strategies for therapeutic intervention with TNFα are suggested by the newly defined conformation.

CONCLUSIONS

DEER as a sensitive solution-based biophysical technique has offered data suggesting that it is capable of identifying a previously unknown conformation of TNFα, which is naturally sampled at low frequency. DEER distance distributions have been used to construct a model of this predeoligomerization conformation of the TNFα trimer and show the rotation and tilting of a protomer. The distorted form of TNFα was detected toward the tip region of TNFα, which is the key region for the formation of the trimeric human TNFα, whereas the DEER probe toward the N/C-terminus did not show any change in interprotomer distances. Of particular interest is that movement of one protomer relative to the others results in distortion of one receptor binding interface. This movement may represent natural conformational sampling of the human TNFα trimer, as TNFα "breathes," in a prelude to deoligomerization. To our knowledge, the new model offers opportunities to modulate the biological activity of TNFα through stabilization of the distorted conformation with small molecules, rather than with therapeutic antibodies or receptors.

SUPPORTING MATERIAL

Eight figures and two tables are available at http://www.biophysj.org/biophysj/supplemental/S0006-3495(17)30627-6.

AUTHOR CONTRIBUTIONS

Protein preparation and labeling and structure determination of the spin-labeled protein, P.H.; DEER data collection, analysis, and revisions, W.K.M.; Model construction, M.C.; Concept and Writing, A.D.G.L. and B.C.

ACKNOWLEDGMENTS

The authors thank David M. Dranow (Beryllium) for structure refinement and David Fox, III (Beryllium) for design of the clones and critical evaluation and discussion of the results, Terry Baker (UCB Celltech) for SEC measurements, and Alison Turner (UCB Celltech) for SEC MALS measurements. Professor Jack Freed is credited with suggesting, at the ACERT workshop, Pulse Dipolar ESR Spectroscopy (PDS), and Biomacromolecular Structure and Function: Instrumentation, Methods and Applications, June 2013, the combination of several DEER data sets as a means to assess peak probabilities.

This research used resources of the Advanced Photon Source (APS), a U.S. Department of Energy (DOE) Office of Science User Facility operated for the DOE Office of Science by Argonne National Laboratory under contract no. DE-AC02-06CH11357. W.K.M. is supported by the United Kingdom Engineering and Physical Sciences Research Council (EPSRC) grant No. EP/L011972/1, to the Centre for Advanced Spin Resonance). Use of the LS-CAT Sector 21 was supported by the Michigan Economic Development Corporation and the Michigan Technology Tri-Corridor (grant 085P1000817).

A.D.G.L. holds shares and share options, and B.C. holds share options in UCB.

REFERENCES

1. Carswell, E. A., L. J. Old, …, B. Williamson. 1975. An endotoxin-induced serum factor that causes necrosis of tumors. *Proc. Natl. Acad. Sci. USA.* 72:3666–3670.
2. Curtis, J. R., and J. A. Singh. 2011. Use of biologics in rheumatoid arthritis: current and emerging paradigms of care. *Clin. Ther.* 33:679–707.
3. Wingfield, P., R. H. Pain, and S. Craig. 1987. Tumour necrosis factor is a compact trimer. *FEBS Lett.* 211:179–184.
4. Jones, E. Y., D. I. Stuart, and N. P. C. Walker. 1989. Structure of tumour necrosis factor. *Nature.* 338:225–228.
5. Corti, A., G. Fassina, …, G. Cassani. 1992. Oligomeric tumour necrosis factor α slowly converts into inactive forms at bioactive levels. *Biochem. J.* 284:905–910.
6. Poiesi, C., A. Albertini, …, A. Corti. 1993. Kinetic analysis of TNF-α oligomer-monomer transition by surface plasmon resonance and immunochemical methods. *Cytokine.* 5:539–545.
7. Alzani, R., E. Cozzi, …, V. Rizzo. 1995. Mechanism of suramin-induced deoligomerization of tumor necrosis factor α. *Biochemistry.* 34:6344–6350.
8. He, M. M., A. S. Smith, …, B. C. Cunningham. 2005. Small-molecule inhibition of TNF-α. *Science.* 310:1022–1025.
9. Luzi, S., Y. Kondo, …, P. Holliger. 2015. Subunit disassembly and inhibition of TNFα by a semi-synthetic bicyclic peptide. *Protein Eng. Des. Sel.* 28:45–52.
10. Chan, D. S. H., H. M. Lee, …, D. L. Ma. 2010. Structure-based discovery of natural-product-like TNF-α inhibitors. *Angew. Chem. Int. Ed. Engl.* 49:2860–2864.
11. Choi, H., Y. Lee, …, D.-S. Oh. 2010. Discovery of the inhibitors of tumor necrosis factor α with structure-based virtual screening. *Bioorg. Med. Chem. Lett.* 20:6195–6198.
12. Murdaca, G., F. Spanò, …, F. Puppo. 2016. Immunogenicity of infliximab and adalimumab: what is its role in hypersensitivity and modulation of therapeutic efficacy and safety? *Expert Opin. Drug Saf.* 15:43–52.
13. Leon, L., L. Rodriguez-Rodriguez, …, L. Abasolo. 2016. Long-term drug survival of biological agents in patients with rheumatoid arthritis in clinical practice. *Scand. J. Rheumatol.* 45:456–460.
14. Rees, H. 2011. Supply Chain Management in the Drug Industry: Delivering Patient Value for Pharmaceuticals and Biologics. John Wiley & Sons, Hoboken, NJ.
15. Hao, W., and A. Friedman. 2016. Mathematical model on Alzheimer's disease. *BMC Syst. Biol.* 10:108.
16. Jeschke, G. 2012. DEER distance measurements on proteins. *Annu. Rev. Phys. Chem.* 63:419–446.
17. Georgieva, E. R., P. P. Borbat, …, O. Boudker. 2013. Conformational ensemble of the sodium-coupled aspartate transporter. *Nat. Struct. Mol. Biol.* 20:215–221.
18. Hänelt, I., D. Wunnicke, …, D. J. Slotboom. 2013. Conformational heterogeneity of the aspartate transporter Glt(Ph). *Nat. Struct. Mol. Biol.* 20:210–214.
19. Krug, U., N. S. Alexander, …, J. Meiler. 2016. Characterization of the domain orientations of *E. coli* 5′-Nucleotidase by fitting an ensemble of conformers to DEER distance distributions. *Structure.* 24:43–56.
20. Tugarinov, V., V. Kanelis, and L. E. Kay. 2006. Isotope labeling strategies for the study of high-molecular-weight proteins by solution NMR spectroscopy. *Nat. Protoc.* 1:749–754.

21. Kabsch, W. 2010. XDS. *Acta Crystallogr. D Biol. Crystallogr.* 66:125–132.

22. Echols, N., R. W. Grosse-Kunstleve, …, P. D. Adams. 2012. Graphical tools for macromolecular crystallography in PHENIX. *J. Appl. Cryst.* 45:581–586.

23. Emsley, P., and K. Cowtan. 2004. Coot: model-building tools for molecular graphics. *Acta Crystallogr. D Biol. Crystallogr.* 60:2126–2132.

24. Wacker, T., G. A. Sierra, and A. Schweiger. 1992. The concept of FID-detected hole-burning in pulsed EPR spectroscopy. *Isr. J. Chem.* 32:305–322.

25. Bowman, M., A. Maryasov, and Y. Tsvetkov. 2008. Electron Paramagnetic Resonance Studies of Radiation Damage to DNA. Environmental Molecular Sciences Laboratory, Richland, WA.

26. Tait, C. E., and S. Stoll. 2016. Coherent pump pulses in double electron electron resonance spectroscopy. *Phys. Chem. Chem. Phys.* 18:18470–18485.

27. Kurshev, V. V., A. M. Raitsimring, and Y. D. Tsvetkov. 1989. Selection of dipolar interaction by the 2+1 pulse train ESE. *J. Magn. Reson.* 81:441–454.

28. Jeschke, G., V. Chechik, …, H. Jung. 2006. DeerAnalysis2006—a comprehensive software package for analyzing pulsed ELDOR data. *Appl. Magn. Reson.* 30:473–498.

29. Eck, M. J., and S. R. Sprang. 1989. The structure of tumor necrosis factor-α at 2.6 Å resolution. Implications for receptor binding. *J. Biol. Chem.* 264:17595–17605.

30. Yang, Z., M. D. Bridges, …, W. L. Hubbell. 2016. A triarylmethyl spin label for long-range distance measurement at physiological temperatures using T1 relaxation enhancement. *J. Magn. Reson.* 269:50–54.

31. Kalai, T., M. Balog, …, K. Hideg. 1999. Synthesis and reactions of a symmetric paramagnetic pyrrolidine diene. *Synthesis.* 1999:973–980.

32. Borbat, P. P., and J. H. Freed. 2007. Measuring distances by pulsed dipolar ESR spectroscopy: spin-labeled histidine kinases. *Methods Enzymol.* 423:52–116.

33. McCoy, A. J., R. W. Grosse-Kunstleve, …, R. J. Read. 2007. Phaser crystallographic software. *J. Appl. Cryst.* 40:658–674.

34. von Hagens, T., Y. Polyhach, …, G. Jeschke. 2013. Suppression of ghost distances in multiple-spin double electron-electron resonance. *Phys. Chem. Chem. Phys.* 15:5854–5866.

35. McNaught, A. D., and A. Wilkinson. IUPAC. Compendium of Chemical Terminology, ("The Gold Book"), Second Edition: WileyBlackwell, Hoboken, NJ.

36. Schrödinger release 2016–4. MacroModel. Schrödinger, LLC, New York, NY.

37. Clackson, T. 2006. Breaking and entering. *Nat. Chem. Biol.* 2:14–15.

38. Liang, S., J. Dai, …, Z. Lou. 2013. Structural basis for treating tumor necrosis factor α (TNFα)-associated diseases with the therapeutic antibody infliximab. *J. Biol. Chem.* 288:13799–13807.

39. Lee, J. U., W. Shin, …, Y.-S. Heo. 2017. Molecular basis for the neutralization of tumor necrosis factor α by certolizumab pegol in the treatment of inflammatory autoimmune diseases. *Int. J. Mol. Sci.* 18:228.

40. Aderka, D., H. Engelmann, …, D. Wallach. 1992. Stabilization of the bioactivity of tumor necrosis factor by its soluble receptors. *J. Exp. Med.* 175:323–329.

41. Ameloot, P., W. Declercq, …, P. Brouckaert. 2001. Heterotrimers formed by tumor necrosis factors of different species or muteins. *J. Biol. Chem.* 276:27098–27103.

42. Steed, P. M., M. G. Tansey, …, B. I. Dahiyat. 2003. Inactivation of TNF signaling by rationally designed dominant-negative TNF variants. *Science.* 301:1895–1898.

43. Polyhach, Y., E. Bordignon, and G. Jeschke. 2011. Rotamer libraries of spin labelled cysteines for protein studies. *Phys. Chem. Chem. Phys.* 13:2356–2366.

44. Tombolato, F., A. Ferrarini, and J. H. Freed. 2006. Dynamics of the nitroxide side chain in spin-labeled proteins. *J. Phys. Chem. B.* 110:26248–26259.

45. Selwood, T., and E. K. Jaffe. 2012. Dynamic dissociating homo-oligomers and the control of protein function. *Arch. Biochem. Biophys.* 519:131–143.

46. Freed, D. M., P. S. Horanyi, …, D. S. Cafiso. 2010. Conformational exchange in a membrane transport protein is altered in protein crystals. *Biophys. J.* 99:1604–1610.

47. Glaenzer, J., M. F. Peter, …, G. Hagelueken. 2017. PELDOR spectroscopy reveals two defined states of a sialic acid TRAP transporter SBP in solution. *Biophys. J.* 112:109–120.

48. Liu, H., L. Dai, …, Q. Yang. 2012. Hydrophobic cavity in C-terminus is essential for hTNF-α trimer conformation. *Biochimie.* 94:1001–1008.

49. Marušič, J., Č. Podlipnik, …, J. Lah. 2012. Recognition of human tumor necrosis factor α (TNF-α) by therapeutic antibody fragment: energetics and structural features. *J. Biol. Chem.* 287:8613–8620.

50. van Schie, K. A., P. Ooijevaar-de Heer, …, T. Rispens. 2016. Therapeutic TNF inhibitors can differentially stabilize trimeric TNF by inhibiting monomer exchange. *Sci. Rep.* 6:32747.

51. Frishman, J. I., C. K. Edwards, 3rd, …, C. A. Dinarello. 2000. Tumor necrosis factor (TNF)-α-induced interleukin-8 in human blood cultures discriminates neutralization by the p55 and p75 TNF soluble receptors. *J. Infect. Dis.* 182:1722–1730.

52. Krippner-Heidenreich, A., I. Grunwald, …, P. Scheurich. 2008. Single-chain TNF, a TNF derivative with enhanced stability and antitumoral activity. *J. Immunol.* 180:8176–8183.

53. Reis, C. R., A. H. van Assen, W. J. Quax, and R. H. Cool. 2011. Unraveling the binding mechanism of trivalent tumor necrosis factor ligands and their receptors. *Mol. Cell. Proteomics.* 10, M110.002808.

54. Boschert, V., A. Krippner-Heidenreich, …, P. Scheurich. 2010. Single chain TNF derivatives with individually mutated receptor binding sites reveal differential stoichiometry of ligand receptor complex formation for TNFR1 and TNFR2. *Cell. Signal.* 22:1088–1096.

55. Fricke, F., S. Malkusch, …, M. Heilemann. 2014. Quantitative single-molecule localization microscopy combined with rule-based modeling reveals ligand-induced TNF-R1 reorganization toward higher-order oligomers. *Histochem. Cell Biol.* 142:91–101.

56. Chan, F. K.-M. 2007. Three is better than one: pre-ligand receptor assembly in the regulation of TNF receptor signaling. *Cytokine.* 37:101–107.

57. Jaffe, E. K. 2005. Morpheeins—a new structural paradigm for allosteric regulation. *Trends Biochem. Sci.* 30:490–497.

58. Lawrence, S. H., and E. K. Jaffe. 2008. Expanding the concepts in protein structure-function relationships and enzyme kinetics: teaching using morpheeins. *Biochem. Mol. Biol. Educ.* 36:274–283.

59. Byun, S., Y. L. Sinskey, …, A. J. Grodzinsky. 2013. Transport and binding of tumor necrosis factor-α in articular cartilage depend on its quaternary structure. *Arch. Biochem. Biophys.* 540:1–8.

60. Friebe, A., and H.-D. Volk. 2008. Stability of tumor necrosis factor α, interleukin 6, and interleukin 8 in blood samples of patients with systemic immune activation. *Arch. Pathol. Lab. Med.* 132:1802–1806.

61. Robak, T., A. Gladalska, and H. Stepień. 1998. The tumour necrosis factor family of receptors/ligands in the serum of patients with rheumatoid arthritis. *Eur. Cytokine Netw.* 9:145–154.

62. Gabizon, R., and A. Friedler. 2014. Allosteric modulation of protein oligomerization: an emerging approach to drug design. *Front Chem.* 2:9.

63. Derewenda, U., Z. Derewenda, …, D. Swenson. 1989. Phenol stabilizes more helix in a new symmetrical zinc insulin hexamer. *Nature.* 338:594–596.

64. Hammarström, P., R. L. Wiseman, …, J. W. Kelly. 2003. Prevention of transthyretin amyloid disease by changing protein misfolding energetics. *Science.* 299:713–716.